A reduced order model to analytically infer atmospheric CO_2 concentration from stomatal and climate data

Wilfried Konrad[a,b,*], Gabriel Katul[c], Anita Roth-Nebelsick[d], Michaela Grein[d]

[a]*Department of Geosciences, Faculty of Science, University of Tübingen, Hölderlinstrasse 12, D-72074 Tübingen, Germany*
[b]*Technical University of Dresden, Institute of Botany, Zellescher Weg 20b, D-01062 Dresden, Germany*
[c]*Nicholas School of the Environment, Box 90328, Duke University, Durham, NC 27708-0328, U.S.A*
[d]*State Museum of Natural History Stuttgart, Rosenstein 1, D-70191 Stuttgart, Germany*

Abstract

To address questions related to the acceleration or deceleration of the global hydrological cycle or links between the carbon and water cycles over land, reliable data for past climatic conditions based on proxies are required. In particular, the reconstruction of palaeoatmospheric CO_2 content (C_a) is needed to assist the separation of natural from anthropogenic C_a variability and to explore phase relations between C_a and air temperature T_a time series. Both T_a and C_a are needed to fingerprint anthropogenic signatures in vapour pressure deficit, a major driver used to explain acceleration or deceleration phases in the global hydrological cycle. Current approaches to C_a reconstruction rely on a robust inverse correlation between measured stomatal density in leaves (ν) of many plant taxa and C_a. There are two methods that exploit this correlation: The first uses calibration curves obtained from extant species assumed to represent the fossil taxa, thereby restricting the suitable taxa to those existing today. The second is a hybrid eco-hydrological/physiological approach that determines C_a with the aid of systems of equations based on quasi-instantaneous leaf-gas exchange theories and fossil stomatal data collected along with other measured leaf anatomical traits and parameters. In this contribution, a reduced order model (ROM) is proposed that derives C_a from a single equation incorporating the aforementioned stomatal data, basic climate (e.g. temperature), estimated biochemical parameters of assimilation and isotope data. The usage of the ROM is then illustrated by applying it to isotopic and anatomical measurements from three extant species. The ROM derivation is based on a balance between the biochemical demand and atmospheric supply of CO_2 that leads to an explicit expression linking stomatal conductance to internal CO_2 concentration (C_i) and C_a. The resulting expression of stomatal conductance from the carbon economy of the leaf is then equated to another expression derived from water vapour gas diffusion that includes anatomical traits. When combined with isotopic measurements for long-term C_i/C_a, C_a can be analytically determined and is interpreted as the time-averaged C_a that existed over the life-span of the leaf. Key advantages of the proposed ROM are: 1) the usage of isotopic data provides constraints on the reconstructed atmospheric CO_2 concentration from ν, 2) the analytical form of this approach permits direct links between parameter uncertainties and reconstructed C_a, and 3) the time-scale mismatch between the application of instantaneous leaf-gas exchange expressions constrained with longer-term isotopic data is reconciled through averaging rules and sensitivity analysis. The latter point was rarely considered in prior reconstruction studies that combined models of leaf-gas exchange and isotopic data to reconstruct C_a from ν. The proposed ROM is not without its limitations given the need to a priori assume a parameter related to the control on photosynthetic rate. The work here further explores immanent constraints for the aforementioned photosynthetic parameter.

Keywords: carbon isotope composition; eco-hydrology; leaf gas exchange;paleoclimate; photosynthesis; stomatal density; time-average

1. Introduction

It has been known for some time now (Allen and Ingram 2002; Held and Soden 2006; Katul et al. 2012) that long-term changes in atmospheric CO_2 concentrations (C_a) and concomitant air temperature (T_a) alter the long-term balance between global precipitation P_g and evaporation E_g as:

$$\frac{\Delta P_g}{P_g} = \frac{\Delta E_g}{E_g}, \tag{1}$$

where ΔP_g and ΔE_g signify the climate-induced precipitation and evaporation changes due to changes in C_a and T_a, respectively. When representing $E_g = \gamma\, VPD$ (γ denotes a bulk transfer coefficient to water vapour and is a function of wind speed, C_a and T_a, VPD is the vapour pressure deficit), the acceleration ($\Delta P_g > 0$) or deceleration ($\Delta P_g < 0$) of the global hydrological cycle can be reasonably constrained by

$$\frac{\Delta P_g}{P_g} = \frac{\Delta \gamma}{\gamma} + \frac{\Delta VPD}{VPD}. \tag{2}$$

The $VPD = e^*(T_a)(1 - RH)$ is governed by the saturation vapour pressure ($e^*(T_a)$, given by the Clausius-Clayperon equation) and air relative humidity (RH) that appears to be robust to large climatic changes. A few approximations described elsewhere (Katul et al. 2012, especially their Figure 2) result in $\Delta VPD/VPD \approx 0.0675\, \Delta T_a$. Climate simulation estimates of $\Delta P_g/P_g$ appear to be a factor of 2 smaller than estimates based only on $\Delta VPDVPD$ (i.e. ignoring $\Delta\gamma/\gamma$) prompting interest in how this quantity is altered by changes in atmospheric CO_2 (past and future) over land and oceans. Over land, inferring $\Delta\gamma/\gamma$ is particularly complicated by the fact that the plant component of γ impacts and is impacted by C_a at a broad range of time scales. This complication may be turned around into an advantage when attempting reconstruction of past C_a, which is fraught with much more uncertainty when compared to its ΔT_a counterpart. In fact, a solid estimation exists and summarized by the IPPC Fourth Assessment Report that covered some 14 reconstruction methods for ΔT_a that are all roughly converging. It is, however, more difficult to obtain sound data for the past C_a (Jordan (2011)) as needed to assess past trends in the hydrological cycle or indirect expressions of it such as the time-evolving phase relation between ΔT_a and C_a. While all aspects of this problem remain well beyond the scope of a single study, reconstruction of global C_a from various proxies that include stomatal data of fossil plants continues to be a subject of inquiry (Beerling and Chaloner 1992, 1993a; Beerling and Woodward 1996; Rundgren and Beerling 1999; Wagner et al. 1999; Royer 2001; Royer et al. 2001; Crowley and Berner 2001; Haworth et al. 2005; Kürschner et al. 2008; Grein et al. 2013; Steinthorsdottir et al. 2013; Franks et al. 2014; Maxbauer et al. 2014). Specifically, what is often disputed are the uncertainties in C_a associated with reconstruction efforts using fossil plants (Poole et al. 1996; Franks et al. 2014), which as shown here can benefit from imposition of eco-hydrological and physiological constraints and constitutes the main novelty of this contribution.

The basic premise to all reconstruction schemes utilizing anatomical stomatal measurements is a robust negative correlation between stomatal density ν and C_a that is often observed on extant plants (either experimentally or with herbarium material). While other factors modulate the rate of change of ν with C_a,

*Corresponding author

Email addresses: wilfried.konrad@uni-tuebingen.de (Wilfried Konrad), gaby@duke.edu (Gabriel Katul), anita.rothnebelsick@smns-bw.de (Anita Roth-Nebelsick), michaela.grein@smns-bw.de (Michaela Grein)

the robustness of the negative correlation between these two variables appears in numerous species (Royer 2001). In fact, Woodward (1987) demonstrated that more than 67% reduction in ν occurs due to C_a increases from 280 ppm to 340 ppm in arboreal species collected over a 200 year period. The original reconstruction technique was based on calibration curves obtained from extant taxa showing a change in ν with increasing C_a. These curves are then applied to fossil data sets where measured changes in ν is used to infer C_a. Using such calibration curves is limited to fossil material belonging to still extant taxa and extrapolations beyond the calibration conditions can be questionable (Beerling 1999). This limitation prompted interest in alternative methods that are mechanistic yet do not *a priori* assume a negative correlation between ν and C_a and frame the scope here.

The basic premise behind the mechanistic eco-hydrological-physiological approaches is that if a negative correlation between ν and C_a exists, it must be attributed to an adaptation of the plant gas exchange system to the availability of atmospheric CO_2. Some studies refute this claim (Bettarini et al. 1998) but many others support it (see e.g. Peñuelas and Matamala 1990; Beerling et al. 1993; McElwain and Chaloner 1995; Wagner et al. 1996; Hetherington and Woodward 2003). Short-term exposure (several years) of plants to changing C_a have minor to no impact on ν as demonstrated by a number of Free Air CO_2 Enrichment (FACE) experiments, gradient-type chamber experiments, or field studies (Malone et al. 1993; Estiarte et al. 1994; Reid et al. 2003). Hence, reconstruction of C_a from ν cannot be explored from short-term manipulation experiments that do not allow long-term evolutionary adaptation. To link ν and C_a mechanistically, models of plant gas exchange that connect the supply of atmospheric CO_2 to the photosynthetic demand are required. The supply side is commonly represented by Fick's law of gas diffusion through stomates and the biochemical photosynthetic demand side is represented by the widely used photosynthesis model of Farquhar et al. (1980). During the last years, efforts were made to estimate C_a from fossil stomatal data directly by using such balance between supply and demand for atmospheric CO_2 (Konrad et al. 2008; Franks et al. 2014). The rationale for developing these models are 1) to ensure the reconstruction method is independent from the stratigraphic range of extant taxa, 2) to allow such reconstruction to utilize other data sources such as isotopic measurements (e.g. $\delta^{13}C$) for constraining C_a (Van De Water et al. 1994), and 3) to explore the eco-physiological basis for the emergence of stomatal density responses to increased atmospheric CO_2. While such models do not address all aspects of the sought-after $\Delta\gamma/\gamma$, they do offer a novel eco-hydrological perspective on how to constrain some of its components on time scales commensurate with plant evolution.

It should be mentioned that besides ν, the size of the stomatal pore can change during evolution (Franks and Beerling 2009; de Boer et al. 2016). Thus, adjustment of pore size is perhaps a further adaptive element to fine-tune the gas exchange apparatus to shifting CO_2 (Assouline and Or 2013, 2015; Roth-Nebelsick et al. 2012). Stomatal mechanics also varies among plant groups, which may also constrain guard cell size (Franks and Farquhar 2007). It is therefore necessary to obtain the stomatal pore length above and beyond ν when modeling gas exchange using measured leaf anatomical traits. Models describing the effects of increased C_a on ν and gas exchange can be complex depending on the manifold of parameters and processes considered. Within the confines of the C_a reconstruction problem here, model complexity cannot be divorced from available parameters, fossil data, and the stratigraphic age of the material. In this contribution, a reduced order model (ROM) resulting in a single-equation that can be used to analytically infer C_a from stomatal data of C_3-plants (including ν), leaf carbon isotope data and basic climatic conditions is proposed and tested. This ROM is based on approximations to a detailed model linking the soil-plant-atmosphere system described elsewhere (Konrad et al. 2008) but where the measurable macroscopic properties of this system (or order parameters) are substantially reduced without significant loss in accuracy with regards to the inference of C_a. The usage of the term ROM here differs from its popular form used in computational

physics, where a phase-space of a high-dimensional model can be reconstructed using lower-order modes derived from a projection (e.g. proper-orthogonal decomposition). However, the definition here retains the original intent of ROM, which is a reduction in degrees of freedom leading to an approximation of a high-dimensional model covering many aspects of the soil-plant-atmosphere system.

The development of the ROM approach serves two purposes: 1) it provides an analytical foresight that tracks propagation of measurement uncertainties into uncertainties of reconstructed C_a, 2) it exploits the use of isotopic data to constrain reconstructed C_a independent of the anatomical features of the leaf stomata (e.g. stomatal density, aperture, depth, etc...). However, the use of such isotopic data is partly hindered by the inherent time averaging associated with such measurements, which are on the order of several days to time scales commensurate with the life-span of a leaf. To overcome this limitation, the instantaneous equations describing leaf gas exchanges of water vapour and CO_2 must be time-averaged over an interval comparable to the averaging time scale associated with isotopic measurements. Hence, one of the novel outcomes of this work is an exploration of this time-scale mismatch issue between isotopic measurements and leaf-gas exchange equations within the confines of the proposed ROM approach. The latter point is rarely considered (analytically) in prior atmospheric CO_2 concentration reconstruction studies that combined models of leaf-gas exchange and isotopic data (Franks et al. 2014).

2. The model

The diffusion of CO_2 from the atmosphere into leaves is driven by assimilation consuming CO_2 within the chloroplast while leaf transpiration occurs due to the humidity difference between the atmosphere and the near-saturated leaf interior. Both assimilation A and transpiration E rates depend on leaf conductance g that is primarily controlled by stomatal conductance. This assumption means that boundary layer and mesophyll conductances are large when compared to stomatal conductance, which is plausible for inferring reconstructed atmospheric CO_2 concentration over long time scales. Because of the low Reynolds number associated with such gas transport, Fick's law of diffusion can be applied to describe the atmospheric supply of CO_2 into and loss of water from leaves. Conventionally, these gas exchange equations are given as

$$A = g\,(C_a - C_i) \tag{3}$$

$$E = ag\,(w_{sat} - w_a), \tag{4}$$

where C_i is the leaf internal CO_2 concentration, w_{sat} is the leaf internal air humidity, taken as the saturation value for water vapour concentration in air and w_a is the leaf external air humidity. The parameter $a = D_{CO_2}/D_{H_2O} = 1.6$ is the ratio of the molecular diffusional constants of water vapour and CO_2 in air (see also Table 1 for a short summary of the variables). The assimilation of C_3-plants can be described by the Farquhar photosynthesis model (Farquhar et al. 1980, 2001). When this model is used in conjunction with stationary conditions (i.e. all CO_2-molecules diffusing into the leaf interior are finally assimilated), the atmospheric supply of CO_2 into the leaf must be balanced by the assimilation rate given as

$$A = q\,\frac{C_i - \Gamma}{C_i + K} - R_d. \tag{5}$$

The biochemical parameters associated with the photosynthetic demand in equation (5) are as follows: q is carboxylation limited by Rubisco or RuBP regeneration rate, K is a parameter containing Michaelis-Menten constants of carboxylation and oxygenation, Γ is the CO_2 compensation point and R_d is the mitochondrial respiration rate (for details see Konrad et al. 2008; Vico et al. 2013). The dependence of the biochemical parameters q, Γ, K and R_d on air temperature T is described by relations derived in Bernacchi et al. (2003).

Table 1: The model parameters together with their dimensions. The calculated parameters are unknown quantities to be determined by the models. When representing model input to Figures 1, 2 and 3, numerical values shown here are either used or rescaled to the relevant air temperature.

Quantity [Units]	Explanation	*C. sativa*	*G. biloba*	*P. orientalis*
A [μmol/m^2/s]	Assimilation rate	Calculated	Calculated	Calculated
g [m/s]	Leaf conductance [1]	Calculated	Calculated	Calculated
E [mmol/m^2/s]	Transpiration rate	Calculated	Calculated	Calculated
C_a [mol/m^3]	Atmospheric CO_2 [1]	Calculated	Calculated	Calculated
C_i [mol/m^3]	Leaf internal CO_2 [2]	–	–	–
κ [−]	$\kappa := C_i/C_a$ [3]	0.7118	0.6881	0.7683
D_{CO_2} [m^2/s]	Diffusion constant of CO_2 at $T = 25\,^\circ$C		1.55×10^{-5}	
D_{H_2O} [m^2/s]	Diffusion constant of water vapour at $T = 25\,^\circ$C		2.49×10^{-5}	
a [−]	$a := D_{H_2O}/D_{CO_2}$		1.6	
w_a [−]	Leaf external (relative) humidity[4,5]	0.77	0.77	0.77
w_{sat} [−]	Leaf internal (relative) humidity[4]	1.0	1.0	1.0
T [°C]	Temperature (air)[5]	16.5	16.5	16.5
q [μmol/m^2/s]	Carboxylation limited by Rubisco or RuBP at $T = 25\,^\circ$C [6]	58	33	45
K [μmol/m^3]	Contains Michaelis-Menten constants[6]	6926	6926	6926
Γ [μmol/m^3]	CO_2 compensation point[6]	1584	1584	1584
R_d [μmol/m^2/s]	Mitochondrial respiration rate[6]	1.0	1.0	1.0
ν [1/mm^2]	Stomatal density	333	80	165
a_{st} [μm^2]	Stomatal pore area[7,8]	34.7	67.4	58.0
d_{st} [μm]	Depth of stomatal pore[8]	13.7	31.9	19.1
d_{as} [μm]	Thickness of assimilating tissue[8]	83.6	218.0	56.9
τ_{as} [−]	Tortuosity of assimilating tissue[8]	1.571	1.571	1.571
n_{as} [−]	Porosity of assimilating tissue[8]	0.33	0.33	0.33
d_{bl} [mm]	Thickness of boundary layer[9]	2.4	1.6	2.3

Notes:

[1] In the ordinates of Figures 1b, 2b and 3b, g has been converted to units of mol/m^2/s instead of m/s. This is achieved by multiplying the value given in m/s by the factor 42.07 mol/m^3, which is the molar density of air. Similarly, in the abscissa of Figures 1 to 3, C_a has been converted from mol/m^3 to μmol/mol (which is identical to ppm) by multiplying the value given in mol/m^3 by the factor 23 700 (m^3/mol) (μmol/mol).

[2] C_i not contained in the final equations (18)–(22).

[3] Determined from δ^{13}C values (Grein et al. 2011).

[4] Humidity values (air and leaf internal humidity) are necessary only when transpiration rates are to be calculated.

[5] Climate data of Tübingen, Germany (growing sites of the plants were the Botanical Gardens of Tübingen and Hohenheim, close to Tübingen). w_a and T represent average values of those months of the year that belong to the growing season (Grein et al. 2011).

[6] For a list of the data sources for the biochemical demand parameters, see Grein et al. 2011, 2013 and Konrad et al. 2008.

[7] Stomatal pore area is calculated as elliptic shape. Maximum width is determined as the half length of a typical stoma (Grein et al. 2011, 2013).

[8] Values determined from the literature and anatomical preparations (Grein et al. 2011; Konrad et al. 2008).

[9] Leaf boundary layer thickness calculated for 0.5 m/s as a typical wind velocity (Nobel 2005).

The diffusion law also provides a relation between leaf conductance and stomatal density and other leaf anatomical parameters (Parlange and Waggoner 1970; Konrad et al. 2008):

$$g = \frac{\nu a_{st}\, D_{\mathrm{CO}_2}}{\left[d_{bl} + d_{as}\frac{\tau_{as}^2}{n_{as}}\right]\nu a_{st} + d_{st}}, \tag{6}$$

where g is expressed in units consistent with equation (3). ν is — as before — the stomatal density (the basic variable measured), d_{as}, τ_{as}, n_{as} are thickness, tortuosity, and porosity of the assimilation layer, a_{st} is the cross section of the stoma and $d_{st} = d_{st}^{geom} + \sqrt{a_{st}/\pi}$ is a combination of the geometrical thickness d_{st}^{geom} of the stoma and a correction $\sqrt{a_{st}/\pi}$ that is due to the fact that the surfaces of constant CO_2 concentration bulge out from the stomata into boundary layer and intercellular airspace (Nobel 2005). The thickness d_{bl} of the laminar boundary layer attached to the leaf surface depends on the wind velocity v_{wind} and a typical leaf length l. The empirical formula of Nobel (2005) is used here and is given by $d_{bl} = 4 \times 10^{-3}\,(\mathrm{m}/\sqrt{s})\ \sqrt{l/v_{wind}}$ (m and s denote the units meter and second, respectively).

The goal here is to arrive at a relation between ν and C_a using the aforementioned equations assuming stomatal aperture is fully open. A plausibility argument supporting this assumption is that leaves exploit C_a as much as possible but avoid unnecessary construction costs caused by building too many stomata. Hence, the resulting stomatal density is likely to be coordinated with a fully open stomatal aperture. The C_i, however, poses a basic problem since — contrary to the leaf interior humidity — C_i does not represent a known parameter but an unknown quantity that itself varies with A. Thus, a fourth condition is necessary to express C_i in terms of the variables g, A, E and C_a.

It is possible to circumvent this problem by complementing the basic set of equations (3) to (5) with long-term C_i/C_a-ratio that prevailed during the lifetime of the leaf (Konrad 2007). This ratio can be inferred from measurements of δ^{13}C of fossil leaf material because diffusion in the intercellular air spaces and photosynthesis discriminate between the ^{12}C and ^{13}C carbon isotopes (Farquhar et al. 1989). Denoting the C_i/C_a-ratio obtained from measurements by κ, the aforementioned equation is

$$\kappa = \frac{\overline{C_i}}{C_a}. \tag{7}$$

The bar over C_i indicates that κ denotes the ratio between the average value

$$\overline{C_i} := \frac{1}{t_{leaf}} \int_0^{t_{leaf}} C_i(t)\, dt \tag{8}$$

of the fluctuating C_i the leaf has experienced during its lifetime t_{leaf} and the atmospheric CO_2-value C_a, which may be assumed to be time-independent, at least relative to C_i variability over t_{leaf}.

To exploit the isotopic measurements featured in equation (7) and mathematically close the set of equations, equations (3)–(5) must be reformulated so that C_i is replaced by its time-averaged value $\overline{C_i}$ and A be replaced by $\overline{A}$. To achieve this, it is imperative to apply a time-averaging operator on the $A - C_i$ relation given in equation (5). Noting that equation (5) is functionally given as $A = f(C_i)$, then $\overline{A} = \overline{f(C_i)} \neq f(\overline{C_i})$. To link $\overline{A}$ to $\overline{C_i}$, a Taylor series expansion of the expression $A = f(C_i)$ around $\overline{C_i}$ is considered and is given by

$$f(C_i) = f(\overline{C_i}) + \left[\frac{\partial f(C_i)}{\partial C_i}\right]_{\overline{C_i}} \left(C_i - \overline{C_i}\right) + \frac{1}{2}\left[\frac{\partial^2 f(C_i)}{\partial C_i^2}\right]_{\overline{C_i}} \left(C_i - \overline{C_i}\right)^2 + \ldots \tag{9}$$

Upon applying the time-averaging operation to equation (9),

$$\overline{f(C_i)} = f(\overline{C_i}) + \left[\frac{\partial f(C_i)}{\partial C_i}\right]_{\overline{C_i}} \overline{\left(C_i - \overline{C_i}\right)} + \frac{1}{2}\left[\frac{\partial^2 f(C_i)}{\partial C_i^2}\right]_{\overline{C_i}} \overline{\left(C_i - \overline{C_i}\right)^2} + \ldots \tag{10}$$

where $f(\overline{C_i})$ and the partial derivatives in equation (10) are evaluated at $\overline{C_i}$ and are unaffected by the averaging operation provided the integration limits defining the averaging operation (i.e. t_{leaf}) do not vary in time. Furthermore, noting that $\overline{\left(C_i - \overline{C_i}\right)} = 0$ by definition reduces equation (10) to

$$\overline{f(C_i)} = f(\overline{C_i}) + \frac{1}{2}\left[\frac{\partial^2 f(C_i)}{\partial C_i^2}\right]_{\overline{C_i}} \overline{\left(C_i - \overline{C_i}\right)^2} + \ldots \tag{11}$$

where

$$\frac{1}{2}\left[\frac{\partial^2 f(C_i)}{\partial C_i^2}\right]_{\overline{C_i}} = -q\frac{\Gamma + K}{\left(\overline{C_i} + K\right)^3}. \tag{12}$$

Recalling that $\overline{\left(C_i - \overline{C_i}\right)^2} = \mathrm{Var}\,(C_i)$ is the temporal variance in C_i around its mean state $\overline{C_i}$ and inserting this result into equation (5) yields,

$$\overline{A} = q\,\frac{\overline{C_i} - \Gamma}{\overline{C_i} + K} - R_d - q\,\frac{K + \Gamma}{\left(\overline{C_i} + K\right)^3}\,\mathrm{Var}\,(C_i) + \ldots \tag{13}$$

This result shows that $\overline{A} = \overline{f(C_i)} \approx f(\overline{C_i})$ when the dimensionless quantity R_f given by

$$R_f := \frac{(K + \Gamma)\,\mathrm{Var}\,(C_i)}{\left(\overline{C_i} - \Gamma\right)\left(\overline{C_i} + K\right)^2} \ll 1. \tag{14}$$

It is to be noted that when $\overline{C_i}$ (or C_a) becomes large, $R_f \sim [\mathrm{Var}\,(C_i)] \,/\, \left(\overline{C_i}^3\right)$ and is expected to be small. Proceeding similarly with the stomatal conductance, equation (3) can be solved for g, A is eliminated via equation (5) and the result is expanded with respect to C_i. Application of the averaging procedure defined in equation (8) leads to

$$\begin{aligned}\overline{g} = {} & \frac{q\left(\overline{C_i} - \Gamma\right)}{\left(\overline{C_i} + K\right)\left(C_a - \overline{C_i}\right)} - \frac{R_d}{\left(C_a - \overline{C_i}\right)} \\ & + \left[\frac{q\left(\overline{C_i} - \Gamma\right)}{\left(\overline{C_i} + K\right)\left(C_a - \overline{C_i}\right)^3} + \frac{q\ (K + \Gamma)}{\left(\overline{C_i} + K\right)^2\left(C_a - \overline{C_i}\right)^2} - \frac{q\ (K + \Gamma)}{\left(\overline{C_i} + K\right)^3\left(C_a - \overline{C_i}\right)} - \frac{R_d}{\left(C_a - \overline{C_i}\right)^3}\right]\mathrm{Var}\,(C_i) + \ldots\end{aligned} \tag{15}$$

Averaging equation (4) produces

$$\overline{E} = a\overline{g}\,(w_{sat} - w_a). \tag{16}$$

To estimate the contributions of the last terms in (13) and (15), the "worst case" scenario is first assumed, meaning that $\mathrm{Var}\,(C_i) = \overline{C_i^2} - \overline{C_i}^2$ is near its (theoretical) maximum. This "worst case" is characterized by

two conditions: (1) C_i attains either the highest possible value $C_i = C_a$ or the smallest possible value $C_i = \Gamma$. (2) Each of these two values prevails equally long during the leaf lifetime t_{leaf}. If so, $\overline{C_i} = (C_a + \Gamma)/2$. With the numerical values of K and Γ given in Table 1, the relative contributions of the aforementioned terms amount to $\delta\overline{A}/\overline{A} = 36\,\%$ and $\delta\overline{g}/\overline{g} = 56\,\%$ provided $C_a = 400\,\mu\mathrm{mol/mol}$, and $\delta\overline{A}/\overline{A} = 27\,\%$ and $\delta\overline{g}/\overline{g} = 52\,\%$ for $C_a = 1000\,\mu\mathrm{mol/mol}$. Clearly, these values are not acceptable for physiologically unrealistic limits. When $C_i = C_a$, the supply of atmospheric CO_2 from the atmosphere ceases over $t_{leaf}/2$ making this scenario physiologically impossible. Likewise, with $C_i = \Gamma$, the biochemical demand for CO_2 also ceases and the mitochondrial respiratory term exceeds photosynthesis over $t_{leaf}/2$, which is again physiologically impossible over t_{leaf}.

A more realistic assumption (see e.g. Ehleringer and Cerling 1995; Feng 1998; Katul et al. 2000; Yu et al. 2001; Katul et al. 2003; Cernusak et al. 2013; Katul et al. 2010) is that C_i jumps between $C_i = 0.8\,C_a$ and $C_i = 0.6\,C_a$ (implying $\overline{C_i} = 0.7\,C_a$) over t_{leaf}. This assumption produces much smaller contributions with $\delta\overline{A}/\overline{A} = 1.3\,\%$ and $\delta\overline{g}/\overline{g} = 11.5\,\%$ (for $C_a = 400\,\mu\mathrm{mol/mol}$) and $\delta\overline{A}/\overline{A} = 0.9\,\%$ and $\delta\overline{g}/\overline{g} = 10.6\,\%$ (for $C_a = 1000\,\mu\mathrm{mol/mol}$). Still smaller values of $\delta\overline{A}/\overline{A} < 1\,\%$ and $\delta\overline{g}/\overline{g} < 1\,\%$ result if the jumps between $C_i = 0.8\,C_a$ and $C_i = 0.6\,C_a$ are replaced by a smoother sin-function. If the sin-function oscillates between $C_i = 0.8\,C_a$ and $C_i = 0.6\,C_a$, the resulting variance now scales with 50% of the squared amplitude defined by these two limits instead of the entire squared amplitude (experienced in the jump-case). The more realistic of these numerical examples justify keeping only the leading terms in the expansions (13) to (16).

While humidity has a potential influence, with C_i/C_a decreasing under lower water availability (Cernusak et al. 2013; Prentice et al. 2014; Diefendorf et al. 2010) and implications for changing WUE (Dekker et al. 2016), there is evidence that C_i/C_a values are not or not appreciably affected by variations in C_a (Tu et al. 2004). Expressions (13) and (15) have been derived under the tacit assumption that variations of C_a occur on a time-scale greater than the lifetime of a leaf, t_{leaf}. If one drops this assumption and C_a varies within t_{leaf} expression (13) for the assimilation rate A remains unaffected because it does not depend on C_a. Expression (15) for the leaf conductance g, however, becomes more complex: equation (3) (from which A has been eliminated by means of equation (5)) has now to be expanded in a double Taylor series with respect to (C_i, C_a) around $(\overline{C_i}, \overline{C_a})$ where $\overline{C_a}$ is defined in analogy to equation (8). Consequently, definition (7) has to be modified now to yield $\kappa = \overline{C_i}/\overline{C_a}$. One finds

$$
\begin{aligned}
\overline{g} = {} & \frac{q\left(\overline{C_i}-\Gamma\right)}{\left(\overline{C_i}+K\right)\left(\overline{C_a}-\overline{C_i}\right)} - \frac{R_d}{\left(\overline{C_a}-\overline{C_i}\right)} \\
& + \left[\frac{q\left(\overline{C_i}-\Gamma\right)}{\left(\overline{C_i}+K\right)\left(\overline{C_a}-\overline{C_i}\right)^3} + \frac{q\ (K+\Gamma)}{\left(\overline{C_i}+K\right)^2\left(\overline{C_a}-\overline{C_i}\right)^2} - \frac{q\ (K+\Gamma)}{\left(\overline{C_i}+K\right)^3\left(\overline{C_a}-\overline{C_i}\right)} - \frac{R_d}{\left(\overline{C_a}-\overline{C_i}\right)^3}\right]\left(\overline{C_i^2}-\overline{C_i}^2\right) \\
& + \left[\frac{q\left(\overline{C_i}-\Gamma\right)}{2\left(\overline{C_i}+K\right)^2\left(\overline{C_a}-\overline{C_i}\right)^2} - \frac{q\left(\overline{C_a}+\overline{C_i}-2\Gamma\right)}{2\left(\overline{C_i}+K\right)\left(\overline{C_a}-\overline{C_i}\right)^3} + \frac{R_d}{\left(\overline{C_a}-\overline{C_i}\right)^3}\right]\left(\overline{[C_iC_a]}-\overline{C_i}\,\overline{C_a}\right) \\
& + \left[\frac{q\left(\overline{C_i}-\Gamma\right)}{\left(\overline{C_i}+K\right)\left(\overline{C_a}-\overline{C_i}\right)^3} - \frac{R_d}{\left(\overline{C_a}-\overline{C_i}\right)^3}\right]\left(\overline{C_a^2}-\overline{C_a}^2\right) + \ldots
\end{aligned}
\tag{17}
$$

with $\overline{[C_iC_a]} = (1/t_{leaf})\int_0^{t_{leaf}} C_a(t)\,C_i(t)\,dt$. To calculate numeric values for $\delta\overline{g}/\overline{g}$, the relative contributions of the second order terms in the Taylor expansion (second through fourth line in (17)), it is assumed that both C_a and C_i vary sinusoidally around $\overline{C_a}$ and $\overline{C_i}$, respectively; the corresponding C_i values for mean value and extrema are assumed to amount to 70 % of their C_a counterparts. First, we assume that C_a varies between

the extrema $0.9\,\overline{C_a}$ and $1.1\,\overline{C_a}$. Insertion of $C_a = 400\,\text{ppm}$ implies $\delta\overline{g}/\overline{g} = 0.02\%$ and $C_a = 1000\,\text{ppm}$ implies $\delta\overline{g}/\overline{g} = 0.24\%$. If the extrema between which C_a varies are farther apart, namely at $0.5\,\overline{C_a}$ and $1.5\,\overline{C_a}$, one finds for $C_a = 400\,\text{ppm}$: $\delta\overline{g}/\overline{g} = 0.55\%$ and for $C_a = 1000\,\text{ppm}$: $\delta\overline{g}/\overline{g} = 5.81\%$.

Using the relation $\kappa = \overline{C_i}/\overline{C_a}$ to replace $\overline{C_i}$ in favor of the averaged atmospheric CO_2-concentration $\overline{C_a}$ and the quantity κ, the following set of equations can be derived:

$$\overline{A} = q\,\frac{\kappa\overline{C_a} - \Gamma}{\kappa\overline{C_a} + K} - R_d \tag{18}$$

$$\overline{g} = \frac{q\left(\kappa\overline{C_a} - \Gamma\right)}{\left(\kappa\overline{C_a} + K\right)(1-\kappa)\,\overline{C_a}} - \frac{R_d}{(1-\kappa)\,\overline{C_a}} \tag{19}$$

$$\overline{E} = \frac{q\left(\kappa\overline{C_a} - \Gamma\right) - R_d\left(\kappa\overline{C_a} + K\right)}{\left(\kappa\overline{C_a} + K\right)(1-\kappa)\,\overline{C_a}}\,a\,(w_{sat} - w_a) \tag{20}$$

Clearly, expressions (18) to (20) contain less information than their counterparts (3) to (5) due to the temporal averaging. However, for reconstructing palaeo-CO_2 concentration, this reduced information is not a restriction as secular changes in atmospheric CO_2, not daily or diurnal variations within plants, are needed. For simplicity, the bars over C_a are omitted hereafter. A final step must still be taken to complete the reconstruction of palaeo-CO_2 concentration from information provided by fossil leaves. Equating expressions (19) and (6) and solving for the stomatal density, the ROM is now given by

$$\nu = \xi\,\frac{\kappa\,C_a\,(q - R_d) - (q\Gamma + KR_d)}{\eta\,{C_a}^2\,\kappa\,(1-\kappa) + C_a\left[\eta K(1-\kappa) - \kappa(q - R_d)\right] + (q\Gamma + KR_d)}, \tag{21}$$

where

$$\xi := \frac{d_{st}}{a_{st}\,\beta} \qquad \text{and} \qquad \eta := \frac{D_{\mathrm{CO_2}}}{\beta} \qquad \beta := d_{bl} + d_{as}\,\frac{{\tau_{as}}^2}{n_{as}}. \tag{22}$$

After minor algebraic manipulations (21) reduces to a quadratic polynomial in C_a. One of its two solutions is negative (i.e. unphysical), the other one is given by

$$C_a = -\frac{\psi}{2\varphi} + \frac{\sqrt{\psi^2 - 4\varphi\omega}}{2\varphi} \tag{23}$$

where

$$\varphi := \kappa\,(1-\kappa)\,\nu\eta \qquad \psi := \left[(1-\kappa)\,K\nu\eta - \kappa\,(q - R_d)\,(\xi + \nu)\right] \qquad \omega := (q\Gamma + KR_d)\,(\xi + \nu) \tag{24}$$

This completes the sought-after derivation of the ROM linking C_a to ν subject to the constraints imposed by measured κ.

The quantities on the right hand side of equation (23) can be grouped according to their accessibility (cf. Table 1):

(i) The anatomic parameters ν, d_{st}, a_{st}, d_{as}, n_{as}, τ_{as} and the ratio of ^{12}C and ^{13}C carbon isotopes from which κ is derived can be obtained from (fossil) leaves.

(ii) The biochemical parameters q, K, Γ and R_d have to be determined or assumed from extant plants. In the case of fossil plants, it is essential to obtain a reliable estimate for q from close relatives. In contrast, R_d does not carry much weight in expression (5) and need not be known precisely. The K and Γ appear to be insensitive to plant type and all photosynthetic models assume they are universally valid expressions (Bernacchi et al. 2003).

(iii) The air temperature T (the biochemical parameters q, Γ, K and R_d depend on it) and wind speed v_{wind} (determining the boundary layer thickness d_{bl}) have to be known or determined from independent sources.

It is worth noting that (ii) illustrates an essential difference between the ROM here and the model of Franks et al. (2014). Instead of employing the biochemical parameters q, K, Γ and R_d, the model of Franks et al. (2014) relates the (unknown) assimilation rate A of a fossilised plant to the (known) assimilation rate A_0 of a reference plant. Since assimilation rate and biochemical parameters are connected through the Farquhar photosynthesis model given in expression (5), both approaches employ similar information but in different wrappings.

An 'over-simplified model' (hereafter referred to as OSM) that still recovers the inverse correlation between C_a and ν can now be derived from (21) in the limit of $\Gamma/(\kappa C_a) \ll 1$ and $R_d/\overline{A} \ll 1$. In such a limit,

$$C_a = \left[\frac{q}{(1-\kappa)D_{\mathrm{CO}_2}} \frac{d_{st}}{a_{st}} \right] \frac{1}{\nu} + \left[\frac{q\beta}{(1-\kappa)D_{\mathrm{CO}_2}} - \frac{K}{\kappa} \right]. \tag{25}$$

The OSM explicitly reveals the inverse correlation between C_a and ν (i.e. it has the form $C_a = m \times \nu^{-1} + b_o$). It provides a mechanistic interpretation of the slope (m) and intercept (b_o) when regressing C_a upon ν^{-1} as in Franks and Beerling (2009). These regression statistics can now be unambigiously linked to physiological and anatomical parameters. A notable departure between the OSM and the measurements reported in Franks and Beerling (2009) is that the OSM predicts the dependence between C_a and ν^{-1} to be linear, not exponential — at least when d_{st}/a_{st}, q, and κ do not vary with C_a. The 160 data sets listed in Franks and Beerling (2009) lump multiple species (i.e. multiple q values) grown under different climatic conditions (i.e. air temperature and humidity) and feature data with d_{st}/a_{st} that do vary with C_a (as noted in their study). Furthermore, a part of the a_{st} data reported by Franks and Beerling (2009) is not directly measured and but is indirectly inferred. Hence, a one-to-one comparison with such a large data set cannot be readily conducted here without additional information thereby making such a comparison a suitable topic for future inquiry.

In terms of other anatomical features, the OSM predicts that the ratio d_{st}/a_{st} also scales with C_a, though variations in d_{st}/a_{st} are generally smaller than variations in ν explaining the persistent inverse correlation between C_a and ν. The slope m also appears to be independent of the anatomical properties of the photosynthesizing tissue (i.e. d_{as}, τ_{as} and n_{as}) and boundary-layer thickness (all encoded in β) again partly explaining the robustness of the inverse correlation between ν and C_a. However, m also varies linearly with the main physiological property $q(1-\kappa)^{-1}$. This linearity implies that errors incurred when estimating q translate directly to uncertainties in C_a (i.e. $\delta C_a/C_a = \delta q/q$) at least when $\beta q[D_{\mathrm{CO}_2}(1-\kappa)]^{-1} \gg K/\kappa$.

3. Results and Discussion

To evaluate the proposed ROM and OSM expressions, data from three extant species, *Castanea sativa*, *Ginkgo biloba* and *Platanus orientalis* are used as a case study. These extant species vary by a factor of four in their stomatal density but only some 30% in d_{st}/a_{st}. For these three extant species, the ROM and the OSM expressions are compared to the detailed soil-plant-atmosphere model described in Konrad et al. 2008 so as to explore a wider range of conditions than permitted by the data (usually a single-point on the $\nu - C_a$ curve). The detailed model was successfully used in previous studies (Grein et al. 2011, 2013; de Boer et al. 2011) and tested for the three extant species considered here (Grein et al. 2010, 2011). The comparisons between the ROM, the oversimplified model and the detailed model are featured in Figures 1–3. To illustrate the model behaviour, stomatal density, stomatal conductance, transpiration and assimilation rates are presented

against varying CO_2. Differences between the ROM and the detailed model are small despite some two orders of magnitude variability in C_a (from sub-ambient to super-elevated). In fact, the assimilation rate model comparisons are practically identical for all three extant species. For stomatal densities, stomatal conductances and transpiration rates, differences appear highest for low and sub-ambient C_a – but even such differences remain acceptably low for the purposes of C_a reconstruction. For $C_a \gtrapprox 500$ ppm, the detailed model and the ROM are almost identical across all four variables. The high degree of congruence suggests that for the proposed ROM, long-term κ encodes much of the time integrated effects of stomatal aperture adjustments on photosynthesis and the model is thus suitable for reconstructing palaeoatmospheric CO_2. The OSM over-predicts photosynthesis as expected given that it ignores the mitochondrial respiration rate and the CO_2 compensation point. However, it agrees reasonably with the detailed model for the high C_a regime typical of the Palaeozoic, Mesozoic, and early Cenozoic climates (> 500 ppm). Also, the OSM cannot predict a rapid increase in ν with increasing C_a (i.e. a positive correlation) for sub-ambient C_a as expected. This departure between the ROM and OSM at low C_a should be anticipated. At low C_a, the key assumptions employed in deriving the OSM from the ROM (e.g. ignoring R_d and Γ) are no longer plausible but the inverse correlation between ν and C_a is maintained at all C_a values for the OSM.

4. Model limitations and Caveats

In using the proposed ROM, the same caveats apply as for other model approaches with respect to the correctness of the input data. For instance, the biochemical demand parameters must be 'borrowed' from extant plants and may deviate from those of the fossil plants. While typical ranges of parameters for assimilation can be provided (for mesophytic angiosperm deciduous trees, for example), it is well-known that the associated physiological parameters need not be constant under changing C_a and can be affected by CO_2. For example, the parameters $V_{c,max}$ and J_{max} (needed to determine q in equations (5)–(21)) tend to decrease with increasing C_a, a phenomenon termed acclimation (Ainsworth et al. 2003). It is unknown how severe this effect can be for different species or whether this effect can be readily extrapolated to geologic time scales. Hence, the parameter q encodes all such uncertainty and itself may vary with C_a. Although no attempt is made to include the possible dependence of q on C_a into the ROM presented here, it is worth mentioning that the central equation (21) features model immanent constraints for the photosynthetic parameter q briefly discussed next and elaborated upon in an appendix. To begin with, it is certainly not acceptable if (i) the maxima of the $\nu(C_a)$-curves depicted in Figures 1a, 2a and 3a are smaller than the stomatal density found in the fossilized leaves from which palaeo-CO_2 is to be inferred or if (ii) there exist positive C_a-values for which the $\nu(C_a)$-curves approach infinitely high ν-values. Closer inspection of the mathematical structure of expression (21) allows transforming these two conditions into an admissible range for q and into a corresponding C_a-interval, or, put differently, into a compatibility criterion between stomatal density and palaeo-CO_2(details are given in the appendix).

With regards to the OSM derivation, the slope m of the $\nu - C_a$ relation varies linearly with $q/(1-\kappa)$ and uncertainties in any C_a reconstruction will scale linearly with errors in q. Likewise, the switch between Rubisco and RuBP regeneration rates affecting the specification of q and K of the $A - C_i$ curve adds another source of variance, ignored here. A remedy is to employ a co-limitation model (e.g. Vico et al. 2013) for the $A - C_i$ curve that recovers both limitations in their correct regime in a continuous and smooth manner at the expense of needing simultaneously photosynthetically active radiation (PAR) and air temperature. The same applies to the climate data that affect photosynthesis and transpiration. Again, the parameter q does vary with surface temperature and PAR and averaging rules along with Taylor series expansions around the mean states may be used to account (analytically) for their variability. Also, ignoring any interaction between g and $w_{sat} - w_a$ when time averaging over t_{leaf} may introduce biases in estimates of $\overline{E}$ from $\overline{g}$. Specifically,

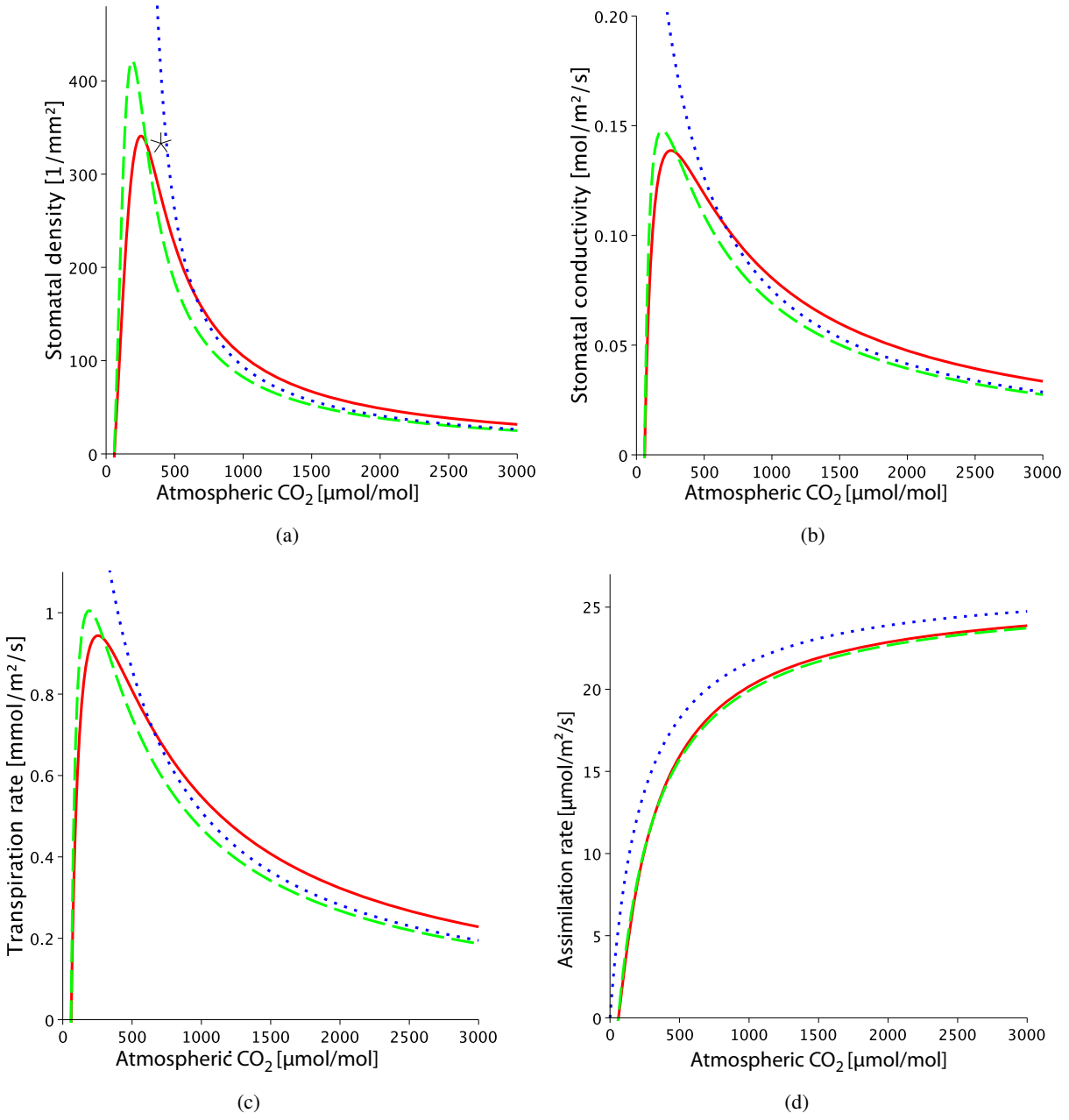

Figure 1: *Castanea sativa*. Detailed model: red, solid lines, ROM: green, broken lines, OSM: blue, dotted lines. The asterisk in subfigure (a) marks the observed values of stomatal density and atmospheric CO_2. Parameter values are as in Table 1.

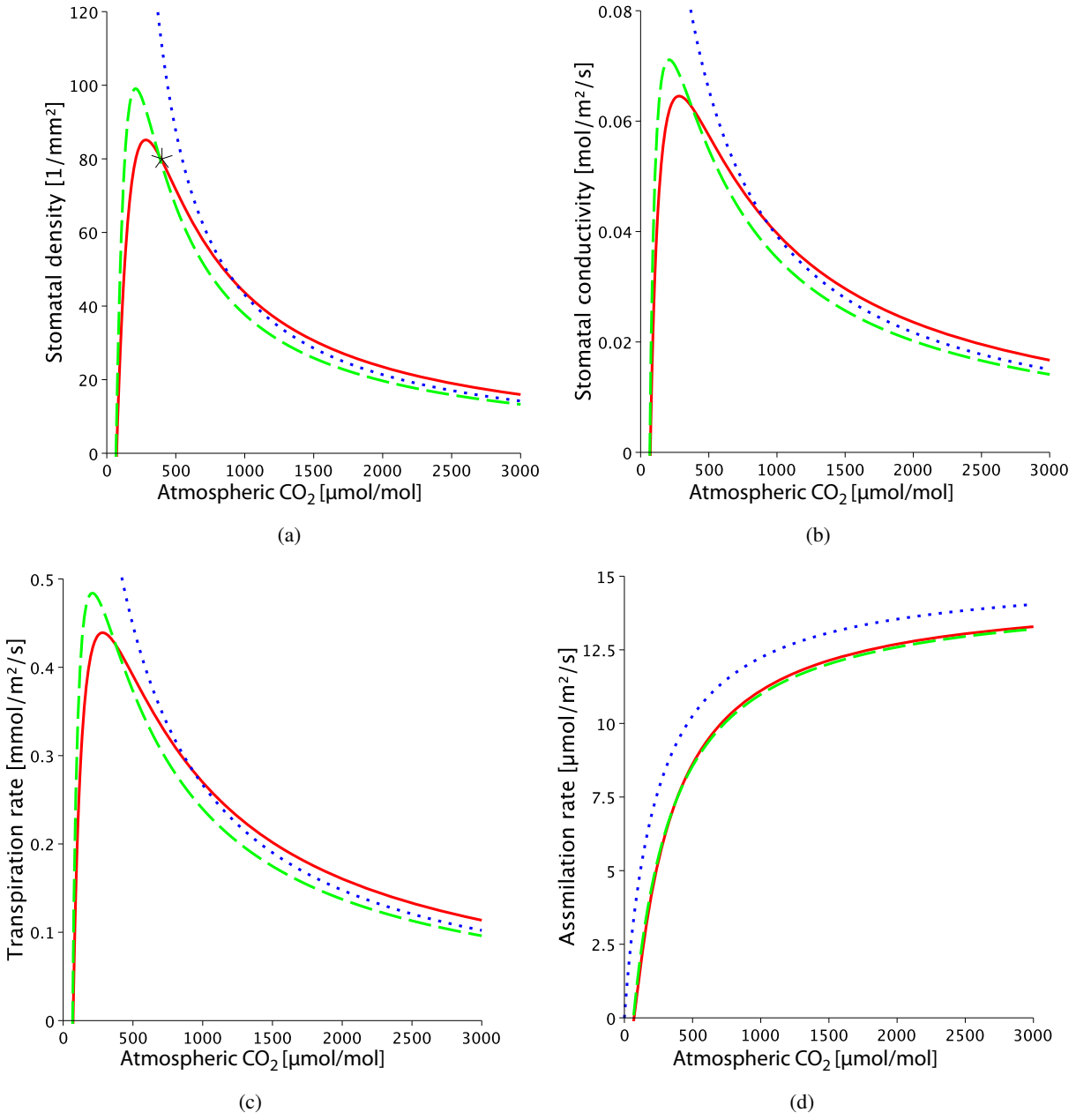

Figure 2: *Ginkgo biloba*. Detailed model: red, solid lines, ROM: green, broken lines, OSM: blue, dotted lines. The asterisk in subfigure (a) marks the observed values of stomatal density and atmospheric CO_2. Parameter values are as in Table 1.

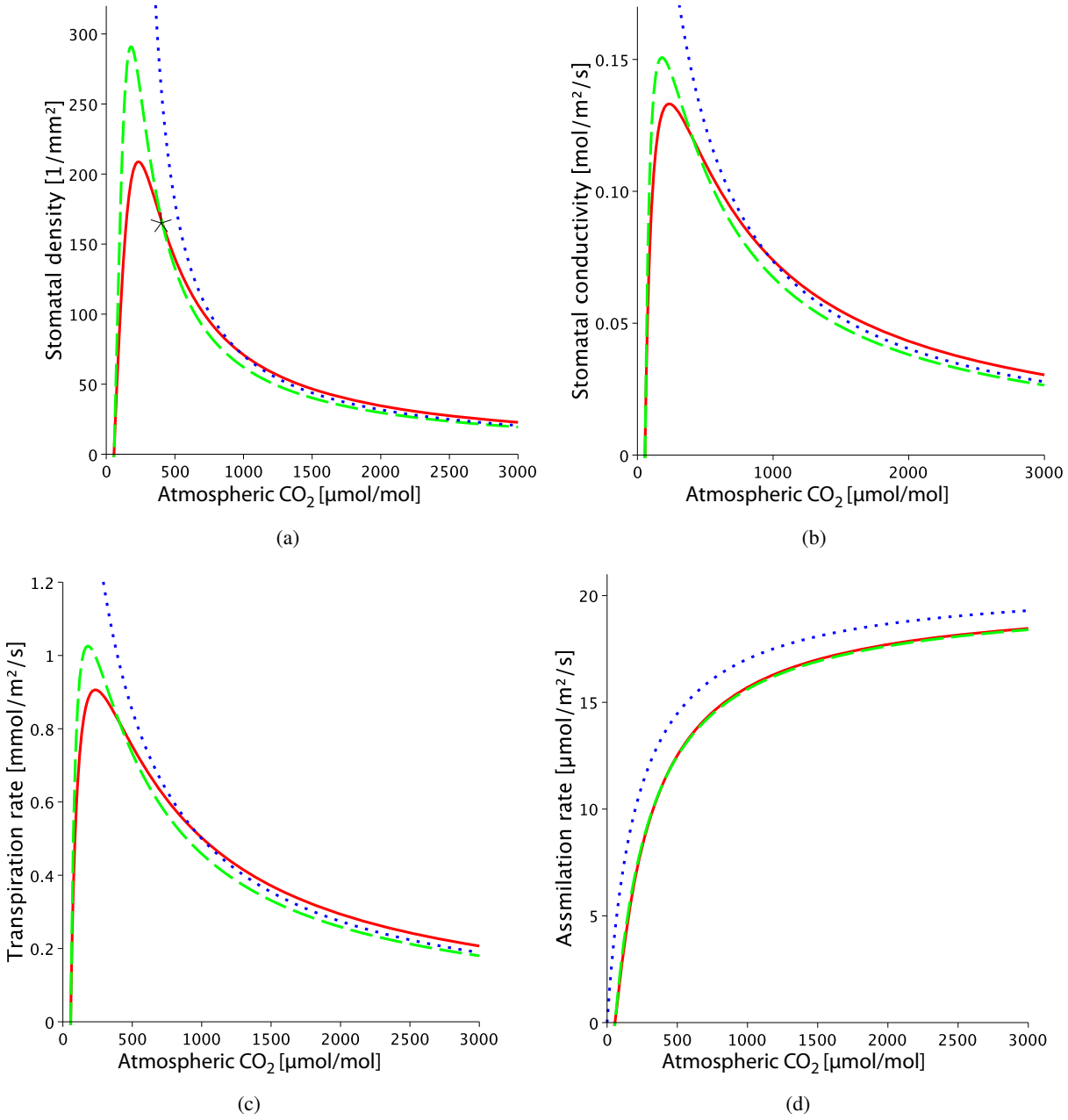

Figure 3: *Platanus orientalis*. Detailed model: red, solid lines, ROM: green, broken lines, OSM: blue, dotted lines. The asterisk in subfigure (a) marks the observed values of stomatal density and atmospheric CO_2. Parameter values are as in Table 1.

stomatal optimization theories (e.g. Katul et al. 2009, 2010) predict that g scales with $(w_{sat} - w_a)^{-1/2}$ and hence $\overline{E} \neq \overline{g} \times \overline{(w_{sat} - w_a)}$ though this latter effect has minor impact on the inference of C_a from ν (not shown here).

To sum up, it is recommended that parameter variations be conducted by inserting the extrema covering the range of parameter uncertainty (see discussions in Konrad et al. 2008; Grein et al. 2011, 2013; Franks et al. 2014) when determining C_a from ν. Additionally, different taxa should be used to assess the consistency of the ROM against other data and detailed model outcomes when time-integrated over t_{leaf}. In doing so, the ROM becomes beneficial because less time-consuming data throughput is required and uncertainty quantification on any parameter (or their interaction with other parameters) can be carried out analytically. A cautionary note is worth repeating here with regards to the causal relation between the derived C_a and ν. There are no model immanent criteria that can attribute the relation between ν and C_a to adaptation of the plant gas exchange system to atmospheric CO_2. This attribution lies outside the scope of the models developed here and is implicitly assumed in the model interpretation. Last, the C_a inferred by the ROM or OSM must be treated as a time-averaged value over the lifetime of the analyzed leaf (order of magnitude ranges from months to year) or the averaging period associated with isotopic measurements of C_i. Implicit to this interpretation is that C_a did not vary appreciably over such time scales.

5. Conclusions

Proxy methods that reconstruct atmospheric CO_2 concentration from stomatal density are urgently needed in climate science to assess historical acceleration/deceleration phases of the global hydrological cycle among other climate dynamics, but uncertainties continue to plague such reconstruction efforts. Over the past decade, a common approach to reconstruct C_a is to use quasi-instantaneous equations describing leaf-gas exchange coupled with carbon isotope composition measurements and stomatal anatomy of fossil leaves as reviewed elsewhere (Franks et al. 2014). The utility of carbon isotope composition measurements reduces the model complexity appreciably by (implicitly) holding constant C_i/C_a over the lifetime of a leaf and offering estimates for its value.

There are a number of open theoretical and practical problems in using such a scheme that are partly addressed here. On the theoretical side, there is a clear mismatch between the time scale over which isotope composition measurements integrate C_i and the time scale over which leaf-gas exchange equations operate. One approach to overcoming this time-scale mismatch is to formally time-average the gas exchange equations so that they become commensurate with the integration time of isotopic measurements. This temporal averaging is necessary because the short-term variations in C_i remain unknown and only $\overline{C_i}$ is available through isotopic measurements. This approach may be reasonable at first glance as variations in the anatomical properties of the leaf (e.g. stomatal density, stomatal pore area, stomatal pore depth, and geometric features of the assimilating tissue) may be ignored compared to other factors over the time-integrated period of C_i.

Because of the non-linearity in the photosynthetic response to variations in C_i, a 'closure problem' arises. That is, to predict the mean photosynthetic rate and C_a from the time-averaged C_i, the higher order moments of C_i (e.g. variances) are needed but these moments cannot be obtained from the aforementioned isotopic measurements. The work here established the necessary conditions as to when these higher-order terms describing C_i variations can be ignored when reconstructing C_a from ν. Because of its analytical form, the proposed ROM can be readily time-averaged thereby bridging the instantaneous leaf-gas exchange equations with the time-integrated isotopic data. Moreover, the necessary conditions as to when the higher-order terms describing C_i variations around its time-integrated value can be ignored when reconstructing C_a from ν have been established. Likewise, the analytical tractability of ROM allows direct links between

parameter uncertainties (in $A-C_i$ curve or biochemical demand function) and the reconstructed atmospheric CO_2 concentration to be established.

Future work will consider variability in mean air temperature (affecting q) and mean air relative humidity explicitly so as to further bound uncertainties in the reconstructed C_a across taxa and fluctuating climatic regimes. Because the limitations on photosynthesis are explicitly considered, it is conceivable that factors other than C_a effects on stomatal density can be delineated. For example, up to 2.5-fold differences in stomatal density values were reported between sunlit and shaded leaves of one *Alnus glutinosa (L.) Gaertn.* tree (Poole et al. 1996). Such difference may be commensurate to or larger than the reported C_a effects on stomatal density for several species (Woodward and Kelly 1995). However, other studies suggest that position in the canopy (e.g. sunlit vs. shaded) as well as local environmental factors on stomatal density variations are small when factoring the large variations in C_a (Chen et al. 2001). The fact that the proposed approach can delineate between Rubisco and RuBP regeneration rate limitations and accounts for C_i/C_a (e.g. Katul et al. 2000, 2003) possibly ameliorates such spatial heterogeneity effects if additional information (e.g. leaf position) are known. Also, explicit accounting for temperature-dependent physiological parameters (e.g. q) admits some model skill in delineating air temperature from C_a effects on stomatal density, shown to be significant in several field studies (Woodward and Bazzaz 1988; Beerling and Chaloner 1993b; Jordan 2011).

The ultimate goal is to arrive at a simplified framework linking C_a to ν, where both exogenous (climatic) and endogenous (photosynthetic and anatomical) system variables are allowed to co-vary when imposing the time-averaging rules. Such a framework can contribute to solving a plethora of hydrological and climate-related problems such as reconstruction of continental scale runoff (Gedney et al. 2006; Betts et al. 2007) and constraining the phase relations between T_a and C_a, among others.

Acknowledgements

G. K. acknowledges support from the National Science Foundation (NSF-EAR-1344703) and the United States Department of Energy (DOE) through the office of Biological and Environmental Research (BER) Terrestrial Ecosystem Science (TES) Program (DE-SC0006967 and DE-SC0011461). This work was supported by a grant of the Volkswagen Foundation to A. R.-N. (Az 87139, project "Ecophysiological signals of plant fossils as indicators of climatic and atmospheric change during the Palaeogene") within the Program "Research in Museums". We also thank the two anonymous reviewers for their valuable comments.

Appendix: Model immanent constraints for the photosynthetic parameter q

As noted in section 4, neither should (i) the maxima of the $\nu(C_a)$-curves be smaller than the stomatal density in the fossilized leaves nor should (ii) a positive C_a-values exist for which the $\nu(C_a)$-curves approach infinitely high ν-values. In what follows, these 'plausibility' conditions are converted into admissible ranges for q and C_a. For simplicity, $R_d = 0$ in what follows, whereupon expression (21) becomes

$$\nu = \frac{\xi\, q\,(\kappa\, C_a - \Gamma)}{\eta\, {C_a}^2\, \kappa\,(1-\kappa) + C_a\,[\eta K(1-\kappa) - \kappa q] + q\Gamma} \tag{26}$$

Theoretical considerations

To reconstruct palaeo-atmospheric CO_2 concentration, a starting point is drawing a (C_a, ν)-coordinate system. Expression (26) (red, green and blue lines in Figure 4a) is then plotted together with the straight line $\nu = \nu_e$ (black line in Figure 4a) that represents the fossil stomatal density. It is envisaged that expression

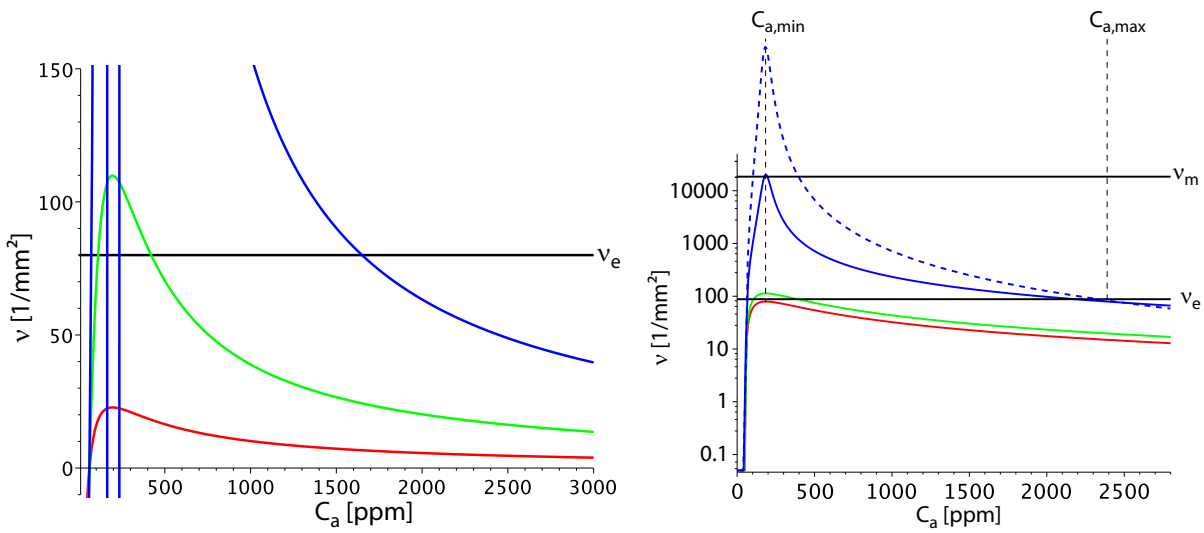

Figure 4: (a) Three versions of expression (26) (red, green and blue curves) and the straight line $\nu = \nu_e$ (black), representing the fossil stomatal density. The red curve does not intersect the line $\nu = \nu_e$; it is therefore (completely) unsuitable to represent a plant whose stomatal density is indicated by the straight black line. The blue curve exhibits singularities (vertical blue lines), it is thus an unsuitable representation of a plant in this area.
(b) Three versions of expression (26) (red, green and blue curves) and the straight lines $\nu = \nu_m$ and $\nu = \nu_e$ (black). $\nu = \nu_e \approx 80/\text{mm}^2$ represents the fossil stomatal density, $\nu = \nu_m = 1/a_{st} \approx 20\,000/\text{mm}^2$ is the theoretical maximum number of stomata that the leaf surface can accommodate. The red and the blue curve originate if the lower and upper boundaries for q as derived in (28) are inserted into relation (26); the green curve represents the q-value measured at a extant relative. (Numerical values are typical for *Ginkgo biloba*.) The blue, broken curve is discussed in the text.

(26) is realized by a green curve in Figure 4a. If so, the higher C_a-value of the (usually) two intersections of the green curve and the black straight line indicates palaeo-CO_2. This scheme may fail under certain instances because:

(i) Expression (26) exhibits singularities (poles) in the range $C_a > 0$, i.e. there exist C_a-values for which ν becomes infinite (blue curve in Figure 4a).

(ii) No intersection point exist between $\nu = \nu_e$ and the graph of expression (26) (red curve in Figure 4a).

This failure occurs when q is assigned an implausible numerical value as may occur if q is borrowed from an extant relative of the fossil plant. Rectifying this error leads to model immanent constraints for the value of q and C_a as discussed next. Figure 4b illustrates how these constraints can be derived: The straight lines $\nu = \nu_e$ and $\nu = \nu_m$ represent the stomatal densities obtained from the fossil plant leaf and from the maximum number of stomata that can be placed on a leaf surface. Ignoring that each stoma is surrounded by guard cells and that some minimum spacing must exist to minimize interferences, etc... this upper limit is given by $\nu_m = 1/a_{st}$ where a_{st} denotes the area of a single stoma. Now, a $\nu(C_a)$ curve that represents a real plant (within the limitations of ROM, i.e. equations (26) resp. (21)) should neither (i) run completely below the $\nu = \nu_e$ line, nor (ii) extend into the area above the $\nu = \nu_m$ line. Notice that the red and blue curves in Figure 4b violate conditions (i) and (ii), respectively (i.e. implausible q), whereas the green curve is consistent with them (q is plausible).

Since ν is a monotonically increasing function of q as evidenced by expression (26), a lower and an upper bound for q can be readily derived by first equating the maximum value of $\nu(C_a^m)$ with ν_e and with ν_m, respectively. Adopting this first step results in

$$C_a^m := \frac{\Gamma + \sqrt{\Gamma^2 + \Gamma K}}{\kappa}. \tag{27}$$

The C_a^m delineates the CO_2 concentration location of the maximum of $\nu(C_a)$. In the second step, the two resulting equations $\nu(C_a^m) = \nu_e$ and $\nu(C_a^m) = \nu_m$ are solved for q, resulting in the interval

$$\frac{(1-\kappa)\,\eta\,\nu_e}{\kappa\,(\xi+\nu_e)}\left(K + 2\Gamma + 2\sqrt{K\Gamma+\Gamma^2}\right) < q < \frac{(1-\kappa)\,\eta\,\nu_m}{\kappa\,(\xi+\nu_m)}\left(K + 2\Gamma + 2\sqrt{K\Gamma+\Gamma^2}\right) \tag{28}$$

with $\nu_m = 1/a_{st}$ setting the theoretical maximum. Thus, any q value within this interval leads to an acceptable $\nu(C_a)$ curve (featured by the green curves in Figure 4b) and precludes 'anomalous' versions of expression (21) (located above the blue or below the red curve in Figure 4b).

The lower boundary of the C_a-interval that corresponds to (28) is given by (27). Its upper counterpart is obtained by first inserting into relation (26) the upper boundary of (28) instead of q, then equating the result with ν_e, and finally solving this equation for C_a. Thus, one finds for the C_a-interval related to (28) the following

$$C_{a,min} < C_a < C_{a,max} \tag{29}$$

with

$$C_{a,min} := \frac{\Gamma + \sqrt{\Gamma^2 + \Gamma K}}{\kappa} \tag{30}$$

and

$$C_{a,max} := -\frac{1}{2\kappa}\left[K - \left(K + 2\Gamma + 2\sqrt{K\Gamma+\Gamma^2}\right)\frac{\nu_m\,(\nu_e+\xi)}{\nu_e\,(\nu_m+\xi)}\right] \tag{31}$$
$$+ \frac{1}{2\kappa}\sqrt{\left[K - \left(K + 2\Gamma + 2\sqrt{K\Gamma+\Gamma^2}\right)\frac{\nu_m\,(\nu_e+\xi)}{\nu_e\,(\nu_m+\xi)}\right]^2 - 4\Gamma\left(K + 2\Gamma + 2\sqrt{K\Gamma+\Gamma^2}\right)\frac{\nu_m\,(\nu_e+\xi)}{\nu_e\,(\nu_m+\xi)}}$$

and with $\nu_m = 1/a_{st}$. The two criteria employed to derive (28) are of a somewhat different quality: the condition leading to the lower boundary $C_{a,min}$ is a necessary condition because the red curve in Figure 4b remains completely below the line $\nu = \nu_e$. In contrast, the condition implying the upper boundary $C_{a,max}$ assumes tacitly that a plant species should be able to thrive in the widest possible range of atmospheric CO_2 levels, encompassing both the all time minimum and maximum of C_a. In a high CO_2 world, a plant species could thrive with a q-value leading to the broken blue curve in Figure 4b, provided C_a does not fall below the value defined by the intersection point of the broken blue curve and the line $\nu = \nu_m$.

The upper boundary in the interval (28) (related to the maximum of the blue curve in Figure 4b) is derived from an unrealistic high stomatal density, $\nu = \nu_m = 1/a_{st} \approx 20\,000/\mathrm{mm}^2$ that reflects the theoretical maximum number of stomata the leaf surface can accommodate, provided $a_{st} \approx 50\,\mu\mathrm{m}^2$. It appears that trees never developed stomatal densities beyond roughly $\nu_m \approx 1000/\mathrm{mm}^2$. Decreasing the distance $\nu_m - \nu_e$ implies narrower q- and C_a-intervals, according to expression (28) and Figure 4b, respectively. To illustrate this, Tables 2 and 3 show numerical results for both cases (values in parentheses are calculated with $\nu_m \approx 1000/\mathrm{m}^2$, the other numbers of the upper boundaries of q and C_a are calculated with $\nu_m = 1/a_{st} \approx 20\,000/\mathrm{mm}^2$).

Numerical examples (extant plants)

Table 2 summarizes the computed intervals from (28) and (29) defining the admissible ranges for q (and C_a). If the upper boundary for q is formed by using $\nu_m = 1/a_{st}$ in (28), $C_a = 400\,\text{ppm}$ lies well inside the ranges of column three (calculated via (29)) and q as given in column four is inside the ranges of column two (calculated via (28)). In contrast, if the upper boundary for q is formed with $\nu_m = 1000/\text{mm}^2$, $C_a = 400\,\text{ppm}$ is again well inside the ranges of column three (notice that in this case the values in parentheses apply). With respect to q, *Platanus orientalis* and *Ginkgo biloba* are also well behaved (i.e. q according to column four is inside the ranges of column two). In the case of *Castanea sativa*, however, the value of column four is approximately equal to the upper boundary of the q-interval given in column two. Actually, it even exceeds the upper boundary by a small amount; but this effect is probably negligible in view of all the other uncertainties. Obviously, the width of the admissible C_a-ranges varies considerably.

Table 2: The ranges for q and C_a calculated using (28) and (29), respectively. As upper boundaries, two values are given: the values in parentheses are obtained by assigning the "maximum stomatal density" the value $\nu_m = 1000/\text{mm}^2$, the other upper boundary values follow from the unrealistic case of $\nu_m = 1/a_{st}$. The q-value in the fourth column is derived by inserting $C_a = 400\,\text{ppm}$ into expression (21). All q-values are normalized to a temperature of 25°C. Other input parameters are as in Table 1.

Species	Range of q [$\mu\text{mol}/\text{m}^2/\text{s}$], according to (28)	Range of C_a [ppm], according to (29)	q [$\mu\text{mol}/\text{m}^2/\text{s}$], at $C_a = 400\,\text{ppm}$
Castanea sativa	$50.3 < q < (64.2)\ 74.2$	$175 < C_a < (419)\ 544$	65.1
Platanus orientalis	$32.6 < q < (53.9)\ 61.3$	$163 < C_a < (604)\ 731$	43.8
Ginkgo biloba	$25.3 < q < (66.7)\ 76.9$	$182 < C_a < (1280)\ 1525$	31.1

Numerical examples (fossil plants)

Table 3 summarizes the computed intervals from (28) and (29) for *Eotrigonobalanus furcinervi* (Late Eocene to the Latest Oligocene, locality Profen), *Metasequoia* sp. (Middle Eocene, locality Napartulik) and *Platanus neptuni* (Late Eocene, localities Borna and Profen). Similarly as in the case of extant plants, the width of the admissible C_a-ranges varies considerably.

Table 3: Ranges for $q = V_{cmax}$ and related CO_2-ranges derived from applying expressions (28) and (29) to fossil leaves of *Eotrigonobalanus furcinervi* (Late Eocene to the Latest Oligocene, locality Profen, Roth-Nebelsick et al. (2012)), *Metasequoia* sp. (Middle Eocene, locality Napartulik, Maxbauer et al. (2014)), *Platanus neptuni* (Late Eocene [Priabonian], locality Borna, Moraweck et al. (2016)) and *Platanus neptuni* (Late Eocene [Priabonian to Bartonian], locality Profen, Moraweck et al. (2016)). The ranges for q and C_a have been calculated using (28) and (29), respectively. As upper boundaries, two values are provided: the values in parentheses are obtained by assigning the "maximum stomatal density" the value $\nu_m = 1000/\text{m}^2$, the other upper boundary values follow via $\nu_m = 1/a_{st}$. All q-values are normalized to a temperature of 25°C.

Species	Range of q [$\mu\text{mol}/\text{m}^2/\text{s}$], according to (28)	Range of C_a [ppm], according to (29)
Eotrigonobalanus furcinervi	$41.5 < q < (45.8)\ 51.5$	$190 < C_a < (324)\ 432$
Metasequoia sp.	$90.3 < q < (152.3)\ 159.9$	$241 < C_a < (1208)\ 1309$
Platanus neptuni (locality Borna)	$51.4 < q < (114.2)\ 139.8$	$193 < C_a < (1108)\ 1436$
Platanus neptuni (locality Profen)	$60.1 < q < (132.3)\ 165.7$	$196 < C_a < (1108)\ 1479$

References

Ainsworth, E. A., Rogers, A., Blum, H., Nösberger, J., Long, S. P., 2003. Variation in acclimation of photosynthesis in *Trifolium repens* after eight years of exposure to Free Air CO_2 Enrichment (FACE). Journal of Experimental Botany 54 (393), 2769–2774.

Allen, M. R., Ingram, W. J., 2002. Constraints on future changes in climate and the hydrologic cycle. Nature 419 (6903), 224–232.

Assouline, S., Or, D., 2013. Plant Water Use Efficiency over Geological Time—Evolution of Leaf Stomata Configurations Affecting Plant Gas Exchange. PloS one 8 (7), e67757.

Assouline, S., Or, D., 2015. Correction: Plant Water Use Efficiency over Geological Time—Evolution of Leaf Stomata Configurations Affecting Plant Gas Exchange. PloS one 10 (4), e0127015.

Beerling, D., 1999. Stomatal density and index: theory and application. Fossil plants and spores: modern techniques. London: Geological Society, 251–256.

Beerling, D., Chaloner, W., Huntley, B., Pearson, J., Tooley, M., 1993. Stomatal density responds to the glacial cycle of environmental change. Proceedings of the Royal Society of London B: Biological Sciences 251 (1331), 133–138.

Beerling, D., Woodward, F., 1996. Palaeo-ecophysiological perspectives on plant responses to global change. Trends in Ecology & Evolution 11 (1), 20–23.

Beerling, D. J., Chaloner, W. G., 1992. Stomatal density as an indicator of atmospheric CO_2 concentration. The Holocene 2 (1), 71–78.

Beerling, D. J., Chaloner, W. G., 1993a. Stomatal density responses of Egyptian *Olea europaea* L. leaves to CO_2 change since 1327 BC. Annals of Botany 71 (5), 431–435.

Beerling, D. J., Chaloner, W. G., 1993b. The impact of atmospheric CO_2 and temperature changes on stomatal density: observation from Quercus robur lammas leaves. Annals of Botany 71 (3), 231–235.

Bernacchi, C. J., Pimentel, C., Long, S. P., 2003. In vivo temperature response functions of parameters required to model RuBP-limited photosynthesis. Plant, Cell and Environment 26, 1419–1430.

Bettarini, I., Vaccari, F. P., Miglietta, F., 1998. Elevated CO_2 concentrations and stomatal density: observations from 17 plant species growing in a CO_2 spring in central Italy. Global Change Biology 4 (1), 17–22.

Betts, R. A., Boucher, O., Collins, M., Cox, P. M., Falloon, P. D., Gedney, N., Hemming, D. L., Huntingford, C., Jones, C. D., Sexton, D. M., et al., 2007. Projected increase in continental runoff due to plant responses to increasing carbon dioxide. Nature 448 (7157), 1037–1041.

Cernusak, L. A., Ubierna, N., Winter, K., Holtum, J. A., Marshall, J. D., Farquhar, G. D., 2013. Environmental and physiological determinants of carbon isotope discrimination in terrestrial plants. New Phytologist 200 (4), 950–965.

Chen, L.-Q., Li, C.-S., Chaloner, W. G., Beerling, D. J., Sun, Q.-G., Collinson, M. E., Mitchell, P. L., 2001. Assessing the potential for the stomatal characters of extant and fossil Ginkgo leaves to signal atmospheric CO_2 change. American Journal of Botany 88 (7), 1309–1315.

Crowley, T. J., Berner, R. A., 2001. CO_2 and Climate Change. Science 292 (5518), 870–872.

de Boer, H. J., Lammertsma, E. I., Wagner-Cremer, F., Dilcher, D. L., Wassen, M. J., Dekker, S. C., 2011. Climate forcing due to optimization of maximal leaf conductance in subtropical vegetation under rising CO_2. Proceedings of the National Academy of Sciences 108 (10), 4041–4046.

de Boer, H. J., Price, C. A., Wagner-Cremer, F., Dekker, S. C., Franks, P. J., Veneklaas, E. J., 2016. Optimal allocation of leaf epidermal area for gas exchange. New Phytologist 210 (4), 1219–1228.

Dekker, S. C., Booth, B. B., Cox, P. M., 2016. Spatial and temporal variations in plant water-use efficiency inferred from tree-ring, eddy covariance and atmospheric observations. Earth System Dynamics 7 (2), 525.

Diefendorf, A. F., Mueller, K. E., Wing, S. L., Koch, P. L., Freeman, K. H., 2010. Global patterns in leaf ^{13}C discrimination and implications for studies of past and future climate. Proceedings of the National Academy of Sciences 107 (13), 5738–5743.

Ehleringer, J. R., Cerling, T. E., 1995. Atmospheric CO_2 and the ratio of intercellular to ambient CO_2 concentrations in plants. Tree Physiology 15 (2), 105–111.

Estiarte, M., Penuelas, J., Kimball, B., Idso, S., LaMorte, R., Pinter, P., Wall, G., Garcia, R., 1994. Elevated CO_2 effects on stomatal density of wheat and sour orange trees. Journal of Experimental Botany 45 (11), 1665–1668.

Farquhar, G., Von Caemmerer, S., Berry, J., 1980. A biochemical model of photosynthetic CO_2 assimilation in leaves of C_3 species. Planta 149, 78–90.

Farquhar, G., Von Caemmerer, S., Berry, J., 2001. Models of Photosynthesis. Plant Physiology 125, 42–45.

Farquhar, G. D., Ehleringer, J. R., Hubick, K. T., 1989. Carbon isotope discrimination and photosynthesis. Annual review of plant biology 40 (1), 503–537.

Feng, X., 1998. Long-term c_i/c_a response of trees in western North America to atmospheric CO_2 concentration derived from carbon isotope chronologies. Oecologia 117 (1-2), 19–25.

Franks, P. J., Beerling, D. J., 2009. Maximum leaf conductance driven by CO_2 effects on stomatal size and density over geologic time. Proceedings of the National Academy of Sciences 106 (25), 10343–10347.

Franks, P. J., Farquhar, G. D., 2007. The mechanical diversity of stomata and its significance in gas-exchange control. Plant Physiology 143 (1), 78–87.
Franks, P. J., Royer, D. L., Beerling, D. J., Van de Water, P. K., Cantrill, D. J., Barbour, M. M., Berry, J. A., Jul 2014. New constraints on atmospheric CO_2 concentration for the Phanerozoic. Geophysical Research Letters, n/a–n/a.
Gedney, N., Cox, P., Betts, R., Boucher, O., Huntingford, C., Stott, P., 2006. Detection of a direct carbon dioxide effect in continental river runoff records. Nature 439 (7078), 835–838.
Grein, M., Oehm, C., Konrad, W., Utescher, T., Kunzmann, L., Roth-Nebelsick, A., 2013. Atmospheric CO_2 from the late Oligocene to early Miocene based on photosynthesis data and fossil leaf characteristics. Palaeogeography, Palaeoclimatology, Palaeoecology 374, 41–51.
Grein, M., Roth-Nebelsick, A., Wilde, V., 2010. Carbon isotope composition of middle Eocene leaves from the Messel Pit, Germany. Palaeodiversity 3, 1–7.
Grein, M., Utescher, T., Wilde, V., Roth-Nebelsick, A., 2011. Reconstruction of the middle Eocene climate of Messel using palaeobotanical data. Neues Jahrbuch für Geologie und Paläontologie-Abhandlungen 260 (3), 305–318.
Haworth, M., Hesselbo, S. P., McElwain, J. C., Robinson, S. A., Brunt, J. W., 2005. Mid-Cretaceous pCO_2 based on stomata of the extinct conifer *Pseudofrenelopsis* (Cheirolepidiaceae). Geology 33 (9), 749–752.
Held, I. M., Soden, B. J., 2006. Robust responses of the hydrological cycle to global warming. Journal of Climate 19 (21), 5686–5699.
Hetherington, A. M., Woodward, F. I., 2003. The role of stomata in sensing and driving environmental change. Nature 424 (6951), 901–908.
Jordan, G. J., 2011. A critical framework for the assessment of biological palaeoproxies: predicting past climate and levels of atmospheric CO_2 from fossil leaves. New Phytologist 192 (1), 29–44.
Katul, G., Ellsworth, D., Lai, C.-T., 2000. Modelling assimilation and intercellular CO_2 from measured conductance: a synthesis of approaches. Plant, Cell & Environment 23 (12), 1313–1328.
Katul, G., Leuning, R., Oren, R., 2003. Relationship between plant hydraulic and biochemical properties derived from a steady-state coupled water and carbon transport model. Plant, Cell & Environment 26 (3), 339–350.
Katul, G., Manzoni, S., Palmroth, S., Oren, R., 2010. A stomatal optimization theory to describe the effects of atmospheric CO_2 on leaf photosynthesis and transpiration. Annals of Botany 105, 431–442.
Katul, G., Palmroth, S., Oren, R., 2009. Leaf stomatal responses to vapour pressure deficit under current and CO_2-enriched atmosphere explained by the economics of gas exchange. Plant, Cell & Environment 32, 968–979.
Katul, G. G., Oren, R., Manzoni, S., Higgins, C., Parlange, M. B., 2012. Evapotranspiration: A process driving mass transport and energy exchange in the soil-plant-atmosphere-climate system. Reviews of Geophysics 50 (3).
Konrad, W., 2007. Functional Anatomy and Biophysical Mechanisms of Fluid Transport in Vascular Plants: Implications for Structural Optimization in Fossil and Extant Plants. Ph.D. thesis, University of Tübingen.
Konrad, W., Roth-Nebelsick, A., Grein, M., 2008. Modelling of stomatal density response to atmospheric CO_2. Journal of Theoretical Biology 253, 638–658.
Kürschner, W. M., Kvaček, Z., Dilcher, D. L., 2008. The impact of Miocene atmospheric carbon dioxide fluctuations on climate and the evolution of terrestrial ecosystems. Proceedings of the National Academy of Sciences 105 (2), 449–453.
Malone, S. R., Mayeux, H. S., Johnson, H. B., Polley, H. W., 1993. Stomatal density and aperture length in four plant species grown across a subambient CO_2 gradient. American Journal of Botany, 1413–1418.
Maxbauer, D. P., Royer, D. L., LePage, B. A., 2014. High Arctic forests during the middle Eocene supported by moderate levels of atmospheric CO_2. Geology 42 (12), 1027–1030.
McElwain, J. C., Chaloner, W. G., 1995. Stomatal density and index of fossil plants track atmospheric carbon dioxide in the Palaeozoic. Annals of Botany 76 (4), 389–395.
Moraweck, K., Grein, M., Konrad, W., Kovar-Eder, J., Kvacek, J., Nenhuis, C., Roth-Nebelsick, A., Stiller, S., Streubig, M., Traiser, C., Utescher, T., Kunzmann, L., 2016. Leaf traits of extinct *Platanus neptuni* (platanaceae): indicators for palaeoenvironment and reliable palaeoclimatic and palaeoatmospheric proxies? Review of Palaeobotany and Palynology (submitted).
Nobel, P. S., 2005. Physicochemical and environmental plant physiology. Academic press.
Parlange, J.-Y., Waggoner, P. E., 1970. Stomatal dimensions and resistance to diffusion. Plant Physiology 46 (2), 337–342.
Peñuelas, J., Matamala, R., 1990. Changes in N and S leaf content, stomatal density and specific leaf area of 14 plant species during the last three centuries of CO_2 increase. Journal of Experimental Botany 41 (9), 1119–1124.
Poole, I., Weyers, J., Lawson, T., Raven, J., 1996. Variations in stomatal density and index: implications for palaeoclimatic reconstructions. Plant, Cell & Environment 19 (6), 705–712.
Prentice, I. C., Dong, N., Gleason, S. M., Maire, V., Wright, I. J., 2014. Balancing the costs of carbon gain and water transport: testing a new theoretical framework for plant functional ecology. Ecology Letters 17 (1), 82–91.
Reid, C. D., Maherali, H., Johnson, H. B., Smith, S. D., Wullschleger, S. D., Jackson, R. B., 2003. On the relationship between stomatal characters and atmospheric CO_2. Geophysical Research Letters 30 (19).

Roth-Nebelsick, A., Grein, M., Utescher, T., Konrad, W., 2012. Stomatal pore length change in leaves of *Eotrigonobalanus furcinervis* (Fagaceae) from the Late Eocene to the Latest Oligocene and its impact on gas exchange and CO_2 reconstruction. Review of Palaeobotany and Palynology 174, 106–112.

Royer, D., 2001. Stomatal density and stomatal index as indicators of paleoatmospheric CO_2 concentration. Review of Palaeobotany and Palynology 114 (1), 1–28.

Royer, D. L., Wing, S. L., Beerling, D. J., Jolley, D. W., Koch, P. L., Hickey, L. J., Berner, R. A., 2001. Paleobotanical evidence for near present-day levels of atmospheric CO_2 during part of the Tertiary. Science 292 (5525), 2310–2313.

Rundgren, M., Beerling, D., 1999. A Holocene CO_2 record from the stomatal index of subfossil *Salix herbacea* L. leaves from northern Sweden. The Holocene 9 (5), 509–513.

Steinthorsdottir, M., Wohlfarth, B., Kylander, M. E., Blaauw, M., Reimer, P. J., 2013. Stomatal proxy record of CO_2 concentrations from the last termination suggests an important role for CO_2 at climate change transitions. Quaternary Science Reviews 68, 43–58.

Tu, T. T. N., Kürschner, W. M., Schouten, S., Van Bergen, P. F., 2004. Leaf carbon isotope composition of fossil and extant oaks grown under differing atmospheric CO_2 levels. Palaeogeography, Palaeoclimatology, Palaeoecology 212 (3), 199–213.

Van De Water, P. K., Leavitt, S. W., Betancourt, J., 1994. Trends in stomatal density and $^{13}C/^{12}C$ ratios of *Pinus flexilis* needles during last glacial-interglacial cycle. Science 264 (5156), 239–243.

Vico, G., Manzoni, S., Palmroth, S., Weih, M., Katul, G., 2013. A perspective on optimal leaf stomatal conductance under CO_2 and light co-limitations. Agricultural and forest meteorology 182, 191–199.

Wagner, F., Below, R., Klerk, P., Dilcher, D. L., Joosten, H., Kürschner, W. M., Visscher, H., 1996. A natural experiment on plant acclimation: lifetime stomatal frequency response of an individual tree to annual atmospheric CO_2 increase. Proceedings of the National Academy of Sciences 93 (21), 11705–11708.

Wagner, F., Bohncke, S. J., Dilcher, D. L., Kürschner, W. M., van Geel, B., Visscher, H., 1999. Century-scale shifts in early Holocene atmospheric CO_2 concentration. Science 284, 1971–1973.

Woodward, F., Bazzaz, F., 1988. The responses of stomatal density to CO_2 partial pressure. Journal of Experimental Botany 39 (12), 1771–1781.

Woodward, F., Kelly, C., 1995. The influence of CO_2 concentration on stomatal density. New Phytologist 131 (3), 311–327.

Woodward, F. I., 1987. Stomatal numbers are sensitive to increases in CO_2 from pre-industrial levels. Nature 327 (6123), 617–618.

Yu, O., Goudriaan, J., Wang, T.-D., 2001. Modelling diurnal courses of photosynthesis and transpiration of leaves on the basis of stomatal and non-stomatal responses, including photoinhibition. Photosynthetica 39 (1), 43–51.